Elimination of Thermomechanical Noise in Piezoelectric Optomechanical Crystals

H. Ramp,[1,*] B.D. Hauer,[1] K.C. Balram,[2] T.J. Clark,[1] K. Srinivasan,[2] and J.P. Davis[1,†]

[1] *Department of Physics, University of Alberta, Canada*

[2] *Center for Nanoscale Science and Technology, National Institute for Standards and Technology, Gaithersburg, USA*

(Dated: December 21, 2018)

Mechanical modes are a potentially useful resource for quantum information applications such as quantum-level wavelength transducers due to their ability to interact with electromagnetic radiation across the spectrum. A significant challenge for wavelength transducers is thermal noise in the mechanical mode, which pollutes the transduced signal with thermal states. In this paper, we eliminate thermomechanical noise in the GHz-frequency mechanical breathing mode of a piezoelectric optomechanical crystal using cryogenic cooling in a dilution refrigerator. We measure an average thermal occupancy of the mechanical mode of only 0.7 ± 0.4 phonons. We further present measurements of the time evolution of the thermal occupancy and quantum optomechanical cooperativity under pulsed optical excitation. These results are a critical step towards using piezoelectric optomechanical crystals in quantum applications.

Quantum information science may have begun with atoms and optical photons, but it has expanded to include numerous experimental platforms that have now demonstrated quantum behavior. Examples of quantum devices now include a wide array of well-controlled natural systems including neutral atoms [1], ions [2, 3], electronic [4, 5] and nuclear spins [6, 7], as well as fabricated systems such as quantum dots [8], superconducting circuits [9–11] and mechanical devices [12–15]. Each system has a unique set of properties that make them advantageous for specific applications: for example, long coherence times make atomic systems a natural candidate for quantum memories [16–19], while the flexible nature of fabrication makes superconducting circuitry ideal for creating quantum processing gates [20]. This has culminated in the vision of hybrid quantum systems that can link multiple sub-systems into complex quantum machines [21, 22].

One major challenge in creating hybrid quantum systems arises from transferring quantum information between the different sub-systems. Photons are the obvious medium for transferring of information as most quantum systems can interact with light, however the relevant wavelength varies widely. This has spurred interest in the development of mechanical wavelength transducers, devices that use photon-phonon interactions to coherently convert photons between different wavelengths while preserving quantum information. Such a mechanical wavelength transducer would consist of a mechanical element coupled to two electromagnetic resonances at the desired input/output wavelengths. State-of-the-art transducers have demonstrated classical wavelength conversion for signals within the optical wavelength range [23–25], within the microwave regime [26, 27], the up-conversion of microwave tones to optical wavelengths [28–30], and the bidirectional conversion of microwave and optical signals [31–33].

Transitioning from the conversion of classical tones to the quantum conversion of single photons is daunting, in part due to the probability of extracting thermal phonons from the mechanical mode instead of the desired quantum state, as outlined in Fig. 1. For this reason, it is important to eliminate thermomechanical noise such that the mechanical resonator is in its ground state, where the number of thermal phonons is less than one. Here, we demonstrate the ground-state cooling of a GHz-frequency mechanical mode of a GaAs optomechanical crystal [34], which has been previously inaccessible with optically measured (as opposed to via microwave) optomechanical devices, reaching an average thermal phonon occupation of $\bar{n}_{\rm th} = 0.7 \pm 0.4$ (95 % confidence interval). Furthermore, using GaAs opens up the possibility of interaction with both optical and mi-

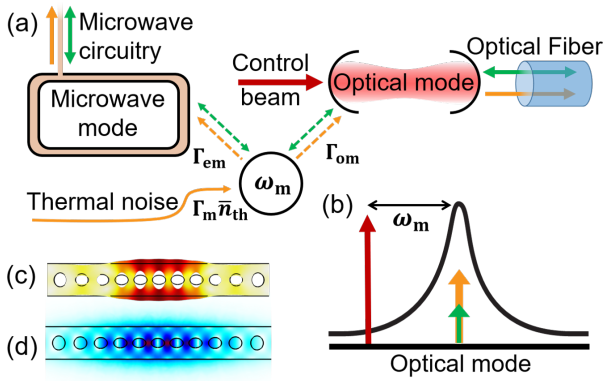

FIG. 1. (a) Schematic of a route to mechanically-mediated wavelength conversion: a mechanical resonator at frequency $\omega_{\rm m}$ is coupled to microwave and optical modes (for example) at rates $\Gamma_{\rm em}$ and $\Gamma_{\rm om}$ respectively, allowing for the bidirectional transduction of a quantum state (green). The mechanical resonator is populated with thermal phonons (orange) at a rate $\Gamma_{\rm m}\bar{n}_{\rm th}$, which are converted into thermal noise photons. (b) A control beam (red) is red-detuned from the optical resonance by one mechanical frequency, allowing conversion between phonons in the mechanical mode and optical photons. (c) Displacement simulation of the GHz-frequency mechanical breathing mode and (d) electric field simulation of the optical mode of an optomechanical crystal.

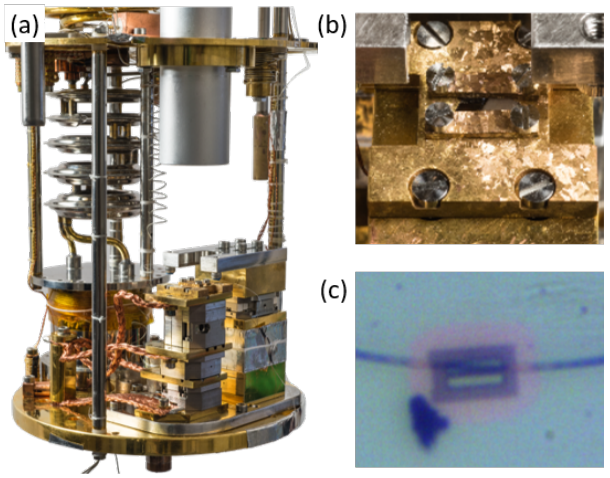

FIG. 2. (a) Base plate of the dilution refrigerator. Devices are mounted in a chip holder, placed on a stack of piezoelectric positioning stages. Copper braids provide thermal coupling between the chip holder and the dilution unit. A high-efficiency dimpled tapered fiber is mounted next to the positioning stack. An optical imaging system [35] above the chip holder allows for real-time optical access to the device to facilitate coupling. (b) Close up of holder with GaAs chip. c) Microscope image of device while coupled to a dimpled tapered fiber.

crowave modes, useful for microwave-to-optical conversion, via piezoelectric coupling.

The elimination of thermomechanical noise in the 2.4 GHz breathing mode of the GaAs optomechanical crystal, engineered to have a 1550 nm optical mode as shown in Fig. 1, is achieved using a carefully designed refrigeration system (shown in Fig. 2 and detailed in Appendix A) to best ensure that the GaAs chip is thermalized to the base plate of the dilution refrigerator. Despite this precaution, low-power optical measurements of the device result in heating of the mechanical mode due to optical absorption, which prevents access to the ground state during continuous wave measurements, as has been previously observed [36, 37]. To circumvent this, we perform pulsed measurements [36, 37], here using an optical heterodyne measurement scheme, shown in Fig. 3a, to optically down-mix and amplify the signal of the mechanical mode. Specifically, we measure the time-dependent integrated power spectral density [38],

$$\int S_V(\omega, t)d\omega = \alpha\bar{n}_{\rm th}(t) + \beta, \qquad (1)$$

which is linearly related to the (time-dependent) number of phonons in the mechanical mode, $\bar{n}_{\rm th}(t)$. Here α is a conversion factor determined by device mechanical properties and the measurement setup, and β represents noise due to temperature-independent measurement imprecision and ground state motion.

The pulsed measurement is performed by setting the measurement laser to the optical resonance frequency $\omega_{\rm c}$, which is split into two equal-length paths by a variable coupler. The signal in the local oscillator arm is modulated by an electro-optic modulator (EOM) driven near V_π to create sidebands at $\omega_{\rm c} \pm \omega_{\rm EOM}$. The signal in the device arm interacts with the optomechanical resonator to create sidebands at $\omega_{\rm c} \pm \omega_{\rm m}$. When mixed at the beamsplitter, the arms beat together to create a signal at $\omega_{\rm m} - \omega_{\rm EOM}$, which we typically set to 30 MHz allowing detection using a low-frequency balanced photodiode and measured in the time domain with a fast analog-digital converter.

During such optical measurement pulses, the number of phonons in the mechanical mode transitions from an initial phonon number $\bar{n}_{\rm th}(t_0)$ to a thermal equilibrium set by the optical absorption heating and the cooling power of the system. The time dependence of this heating can be measured through the time-dependent integrated power spectral density. Figure 3b shows a cartoon of the mechanical power spectral density at three different times during an optical pulse. Behind the spectra, $H(\omega)$ shows the 6.25 MHz bandpass filter that is convolved with the mechanical signal to obtain the mechanical peak area as a function of time. Following the work of Refs. 36 and

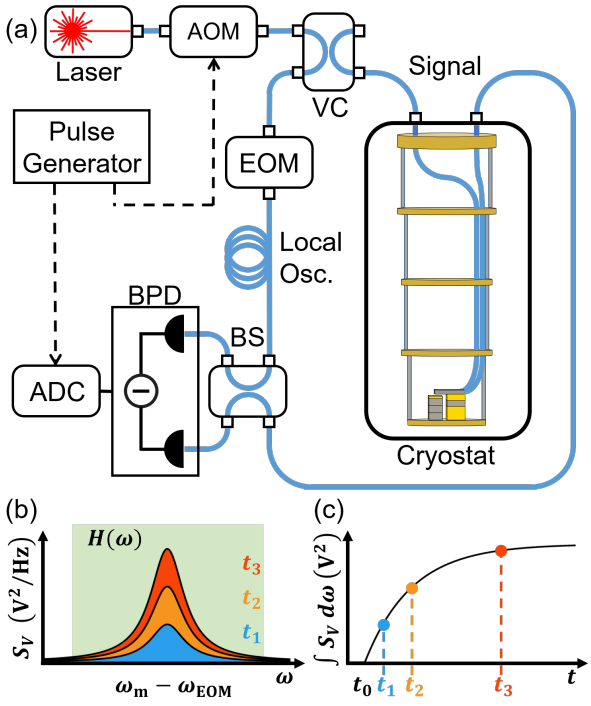

FIG. 3. (a) Simplified schematic of optical heterodyne detection. AOM: acousto-optic modulator, VC: variable coupler, EOM: electro-optic modulator, BS: beamsplitter, BPD: balanced photodiode, ADC: analog-digital converter. (b) Cartoon of frequency-domain mechanical signal at three different times during a pulse. The mechanical signal is convolved with the green filter $H(\omega)$ to obtain (c) the time-dependent mechanical area.

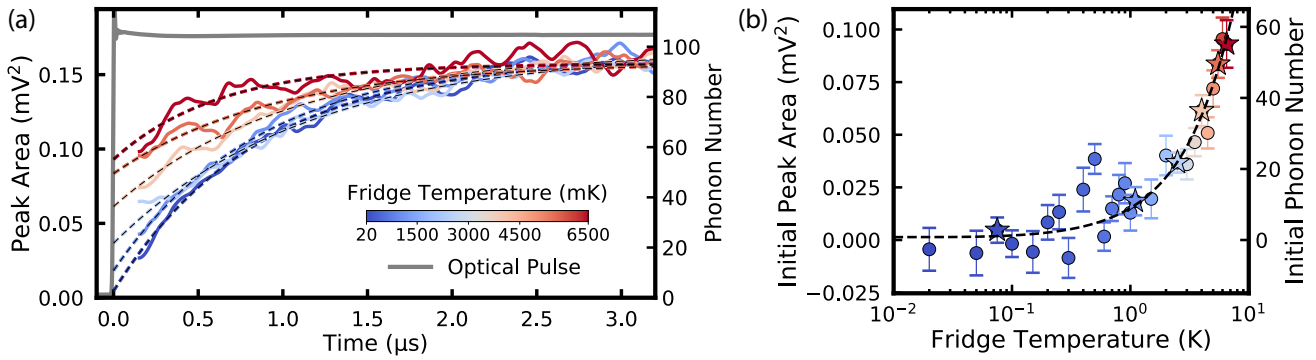

FIG. 4. (a) Heterodyne pulsed measurements showing the thermal noise of the mechanical mode as a function of time. Measurements are truncated to begin at 0.25 μs after the optical pulse (grey) due to the 6.25 MHz bandwidth of the filter function. Fits to Equation (2) (dashed lines) are used to extrapolate the pulses back to $t = 0$. Left axis presents the data in terms of power spectral density peak area with 1.18 mV^2 of imprecision noise removed. Right axis recalibrates the data in terms of phonon number. (b) The peak areas at the onset of the optical pulse, color-coded to match the fridge temperature scale, with stars to denote the example traces from (a). Peak areas from high temperature data $T \geq 1.5$ K are used to calibrate the initial peak area to phonon number. The complete data set is fit to the Bose-Einstein distribution with an offset (black dashed) to determine the average number of phonons in the mechanical mode at 20 mK. Error bars are 95 % confidence intervals derived from these fits.

37, the number of thermal phonons can be modelled as

$$\bar{n}_{\mathrm{th}}(t) = \bar{n}_{\mathrm{th}}(t_0)e^{-\gamma(t-t_0)} + \bar{n}_{\mathrm{eq}}(1 - e^{-\gamma(t-t_0)}), \qquad (2)$$

where γ is a mechanical heating rate and $\bar{n}_{\mathrm{eq}}$ is the number of phonons at thermal equilibrium in the continuous-wave limit. In Fig. 3c, a cartoon of the mechanical peak area $\int S_V(\omega, t)\ d\omega$ is shown according to Equation (2) over the duration of an optical pulse to demonstrate the peak area growth associated with optical heating of the mechanical mode.

By varying the temperature of the thermal reservoir – here the base-plate of the dilution refrigerator – we can track not only the time-dependent phonon number $\bar{n}_{\mathrm{th}}(t)$ but also the inital thermal phonon occupation $\bar{n}_{\mathrm{th}}(t_0)$. We present such pulsed heterodyne measurements of the GaAs optomechanical crystal in Figure 4(a), at dilution refrigerator temperatures between 20 mK and 6.5 K. In these measurements, a 1.5 μW optical laser pulse (set by the minimum power needed for adequate signal-to-noise) is turned on at $t = 0$ and populates the optical mode with $n_{\mathrm{cav}} \approx 230$ photons on a timescale of $2\pi/\kappa = 0.2$ ns. Absorption of photons in the optical mode causes the device to consistently heat to a temperature above 6.5 K regardless of the initial starting temperature. Each trace of the peak area is fit to Equation (2) to extract the initial and final mechanical peak areas, proportional to the phonon occupancy.

At high temperatures, we assume that the device is thermalized to the dilution refrigerator when the measurement begins, which is supported by the linear relationship in Fig. 4b. However, we do not assume that the device is thermalized at millikelvin temperatures, where the GaAs thermal conductivity drops significantly due to T^3 scaling [39]. For this reason only temperatures $T \geq 1.5$ K are used in the calculation of the measurement imprecision. The initial peak areas are fit using Equation (1) to determine the conversion factor, α, as well as the measurement imprecision, β. In Figure 4(b), the initial peak areas are plotted with measurement imprecision removed (left axis) and recalibrated to initial phonon number (right axis) using the conversion factor α. The initial phonon numbers are then fit using a Bose-Einstein distribution to find the thermal offset between the device and the fridge at base temperature. At a fridge temperature of 20 mK we find that the mean phonon occupancy is initially $\bar{n}_{\mathrm{th}} = 0.7 \pm 0.4$ (95 % confidence interval from the fit). This suggests that the mechanical mode is in the ground state 59 % of the time and that the device thermalizes to 0.13 K ± 0.05 K when the fridge thermometry reads 0.02 K.

Applying the calibration to the time resolved measurements in Figure 4(a) shows that the mechanical mode saturates to a thermal occupancy of 95 phonons in 3 μs. To quantify the effect of heating in the context of wavelength conversion, we consider the time dependent quantum cooperativity $\mathcal{C}_{\mathrm{om}}(t) = \Gamma_{\mathrm{om}}/\Gamma_{\mathrm{m}}\bar{n}_{\mathrm{th}}(t)$ [36], where the optomechanical interaction rate is $\Gamma_{\mathrm{om}}/2\pi \approx 0.31$ MHz, and the mechanical damping rate is initially $\Gamma_{\mathrm{m}}/2\pi \approx 83$ kHz (Appendix B), but increases with device temperature – possibly related to two-level systems [40]. The time-dependent phonon number $\bar{n}_{\mathrm{th}}(t)$ is calculated using the fit parameters from Figure 4.

At the onset of the optical pulse, phonons populate the mechanical mode at a rate $\Gamma_{\mathrm{m}}\bar{n}_{\mathrm{th}}(0)/2\pi = 0.058$ MHz, leading to a quantum cooperativity $\mathcal{C}_{\mathrm{om}}(0) = 5.4$. Figure 5, however, shows that the upper bound (assuming Γ_{m} is constant for the duration of the optical pulse) for the quantum cooperativity drops as the thermal phonon

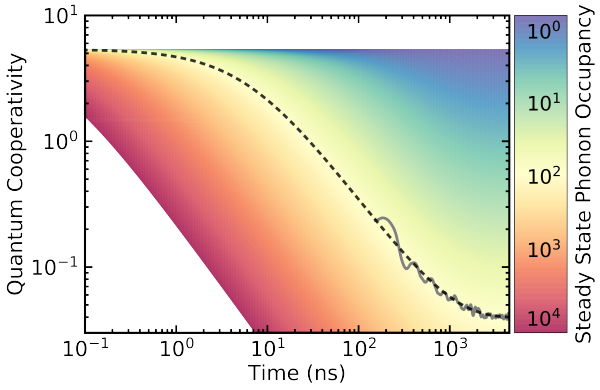

FIG. 5. The upper bound for the quantum cooperativity over the duration of an optical pulse (black dashed), extrapolated from $\bar{n}_{\rm th}(t)$ at 20 mK fridge temperature (grey). In the present experiment our measurement adds 95 phonons on time scales ≥ 3 μs, and would add less than one quanta of noise to a conversion process performed on time-scales ≤ 10 ns, yet one may wish to ask what the quantum cooperativity would be if less heating (or more) were observed. We show the resulting quantum cooperativity from varying levels of added phonons to the mechanical resonator as a background color scale.

number begins to increase. After 25 ns, the quantum cooperativity is reduced to less than 1. To quantify the added thermal noise to the optical signal in a potential wavelength conversion scenario, we consider the steady-state quantum cooperativity of 4×10^{-2} for $t \geq 3$ μs. The added internal thermal noise [23] is only $n_{\rm add} \approx 2/(\bar{n}_{\rm th}^{-1} + \mathcal{C}_{\rm om}) = 39$ quanta. For low-noise conversion of single photon quantum states, the total amount of added noise must be reduced to less than 1, limiting the current device to operations on timescales shorter than 10 ns – which nonetheless may be sufficient for short duration microwave pulse conversion.

The use of optical pulses to determine the phonon occupancy of the GaAs optomechanical crystals reveals several limitations to the cooperativity that require further investigation. First, the mechanical damping rate was expected to be lower than the measured value of $\Gamma_{\rm m}/2\pi = 83$ kHz at millikelvin temperatures. The high damping rate could result from any number of sources, including surface roughness [34], two-level systems [40], or clamping losses [41]. Further studies would be required to elucidate. In addition, Fig. 5 shows that the window for low-noise wavelength conversion is brief, but could be improved by limiting the total number of phonons added by optical absorption. Techniques such as passivating the GaAs surface to reduce roughness and the influence of mid-gap surface states [42] may result in reduced absorption at the surfaces of the optomechanical crystal [43], leading to reduced heating. Gold coating the non-device surface area of the GaAs [37] to increase thermal conductivity may also help by improving the thermal coupling of the devices to the dilution refrigerator. With these improvements, GaAs optomechanical crystals may be capable of achieving $n_{\rm add} < 1$ and $\mathcal{C}_{\rm om} > 1$ required for steady-state low-noise wavelength conversion.

In conclusion, we have used pulsed-optomechanical heterodyne measurements to show that GaAs optomechanical crystals are capable of being cooled to a ground state thermal population of $\bar{n}_{\rm th} = (0.7 \pm 0.4)$ phonons using a dilution refrigerator, while also achieving a quantum cooperativity of $\mathcal{C}_{\rm om} > 1$. Optical absorption causes heating of the mechanical mode resulting in a population of $\bar{n}_{\rm th} = 95$ thermal phonons in the continuous wave limit. Despite this heating, the amount of added noise in a potential wavelength conversion application, $\bar{n}_{\rm add} \approx 39$, is much less than quantum wavelength transducers with MHz-frequency mechanical modes [31]. These results demonstrate GaAs optomechanical crystals are a promising path towards efficient quantum state conversion between microwave and optical light.

ACKNOWLEDGMENTS

This work was supported by the University of Alberta, Faculty of Science; the Natural Sciences and Engineering Research Council, Canada (Grants Nos. RGPIN-04523-16, DAS-492947-16, and CREATE-495446-17); Quantum Alberta; and the Canada Foundation for Innovation. B.D.H. acknowledges support from the Killam Trusts.

APPENDIX A: LOW-TEMPERATURE SETUP

Our low temperature optomechanics setup is designed to allow for flexible optical coupling while also maximizing the thermal connection between the dilution refrigerator and the device. Figure 2(a) is a photograph of the base plate of the dilution refrigerator which demonstrates the optical coupling and cooling systems. A closeup of the chip holder, Figure 2(b), shows the GaAs chip mounted in an annealed copper chip holder that has been gold plated to provide a malleable surface. The chip is screwed in tightly enough to deform the surface of the chip holder, which creates a high surface area mechanical connection for thermal conduction at millikelvin temperatures. The chip holder is connected to flexible copper braids that transfer heat to the base plate of the dilution refrigerator.

The flexibility of the copper braid anchoring system allows the GaAs chip to be freely maneuvered using a 3-axis piezoelectric positioning stack while remaining thermally anchored. This is critical for the dimpled tapered fiber coupling system that allows for optical coupling to any device on the GaAs chip. The optical coupling can be controlled by using the piezoelectric positioning stages to move the device such that the fiber touches differ-

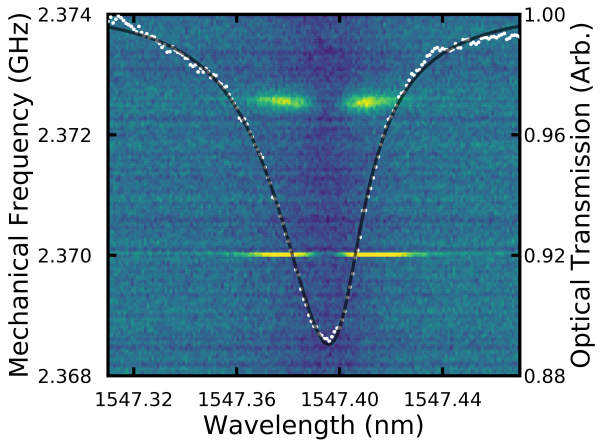

FIG. 6. Wavelength scan of the photonic crystal optical mode (white), fit to a Lorentzian curve (black). The background shows the frequency spectrum at each step of the wavelength scan, with the mechanical resonance and EOM tone.

ent sections of the photonic crystal. Figure 2(c) shows a photonic crystal nanobeam that is optically coupled to a tapered fiber.

APPENDIX B: OPTOMECHANICAL CHARACTERIZATION

Initial characterization of the GaAs photonic crystal nanobeam was performed at 4.2 K using direct detection. In Figure 6, a 1.7 μW tunable telecom laser was used to probe the photonic crystal optical resonance. A Lorentzian fit was used to extract the center frequency $\omega_c/2\pi = 193.7$ THz and the cavity linewidth $\kappa/2\pi = 5.0$ GHz. The optical scan was performed in discrete steps of 1 pm so that the mechanical spectrum could be measured at every laser detuning. The frequency spectrum has two identifiable peaks: the mechanical mode with $Q_m = 1.1 \times 10^3$ at frequency $\omega_m/2\pi = 2.3725$ GHz, and a calibration tone generated by an EOM at $\omega_{\mathrm{EOM}}/2\pi = 2.37$ GHz. The EOM tone is used for phase calibration [44] to calculate the single photon-single phonon optomechanical coupling $g_0/2\pi = 1.3 \pm 0.3$ MHz (at 4.2 K). When the temperature is decreased to the millikelvin regime, the mechanical Q-factor improves to $Q_{\mathrm{m}} = 28,800$. The cooperativity is calculated from the optomechanical interaction rate $\Gamma_{\mathrm{om}} = 4g_0^2 n_{\mathrm{cav}}/\kappa = 2\pi \times 0.31$ MHz, where $n_{\mathrm{cav}} = 230$ is the number of phonons in the optical mode.

* ramp@ualberta.ca
† jdavis@ualberta.ca

[1] M. Saffman, "Quantum computing with atomic qubits and rydberg interactions: progress and challenges," J. Phys. B: At. Mol. Opt. Phys. **49**, 202001 (2016).
[2] R. Blatt and D. Wineland, "Entangled states of trapped atomic ions," Nature **453**, 1008–1015 (2008).
[3] C. Monroe and J. Kim, "Scaling the ion trap quantum processor," Science **339**, 1164–1169 (2013).
[4] R. J. Epstein, F. M. Mendoza, Y. K. Kato, and D. D. Awschalom, "Anisotropic interactions of a single spin and dark-spin spectroscopy in diamond," Nat. Phys. **1**, 94–98 (2005).
[5] R. Hanson, F. M. Mendoza, R. J. Epstein, and D. D. Awschalom, "Polarization and readout of coupled single spins in diamond," Phys. Rev. Lett. **97**, 087601 (2006).
[6] B. E. Kane, "A silicon-based nuclear spin quantum computer," Nature **393**, 133–137 (1998).
[7] L. Childress, M. V. Gurudev Dutt, J. M. Taylor, A. S. Zibrov, F. Jelezko, J. Wrachtrup, P. R. Hemmer, and M. D. Lukin, "Coherent dynamics of coupled electron and nuclear spin qubits in diamond," Science **314**, 281–285 (2006).
[8] Y. Okazaki, I. Mahboob, K. Onomitsu, S. Sasaki, and H. Yamaguchi, "Gate-controlled electromechanical back-action induced by a quantum dot," Nat. Commun. **7**, 11132 (2016).
[9] J. Clarke and F. K. Wilhelm, "Superconducting quantum bits," Nature **453**, 1031–1042 (2008).
[10] R. J. Schoelkopf and S. M. Girvin, "Wiring up quantum systems," Nature **451**, 664–669 (2008).
[11] J. M. Martinis, "Superconducting phase qubits," Quantum Inf. Process. **8**, 81–103 (2009).
[12] A. D. O'Connell, M. Hofheinz, M. Ansmann, Radoslaw C. Bialczak, M. Lenander, Erik Lucero, M. Neeley, D. Sank, H. Wang, M. Weides, J. Wenner, John M. Martinis, and A. N. Cleland, "Quantum ground state and single-phonon control of a mechanical resonator," Nature **464**, 697–703 (2010).
[13] E. E. Wollman, C. U. Lei, A. J. Weinstein, J. Suh, A. Kronwald, F. Marquardt, A. A. Clerk, and K. C. Schwab, "Quantum squeezing of motion in a mechanical resonator," Science **349**, 952–955 (2015).
[14] F. Lecocq, J. B. Clark, R. W. Simmonds, J. Aumentado, and J. D. Teufel, "Quantum nondemolition measurement of a nonclassical state of a massive object," Phys. Rev. X **5**, 041037 (2015).
[15] A. P. Reed, K. H. Mayer, J. D. Teufel, L. D. Burkhart, W. Pfaff, M. Reagor, L. Sletten, X. Ma, R. J. Schoelkopf, E. Knill, and K. W. Lehnert, "Faithful conversion of propagating quantum information to mechanical motion," Nat. Phys. **13**, 1163–1167 (2017).
[16] B. Julsgaard, J. Sherson, J. I. Cirac, J. Fiurášek, and E. S. Polzik, "Experimental demonstration of quantum memory for light," Nature **432**, 482–486 (2004).
[17] A. I. Lvovsky, B. C. Sanders, and W. Tittel, "Optical quantum memory," Nat. Photonics **3**, 706–714 (2009).
[18] C. Simon, M. Afzelius, J. Appel, A. Boyer de la Giroday, S. J. Dewhurst, N. Gisin, C. Y. Hu, F. Jelezko, S. Krll, J. H. Mller, J. Nunn, E. S. Polzik, J. G. Rarity, H. De Riedmatten, W. Rosenfeld, A. J. Shields, N. Skld, R. M. Stevenson, R. Thew, I. A. Walmsley, M. C. Weber, H. Weinfurter, J. Wrachtrup, and R. J. Young, "Quantum memories," Eur. Phys. J. D **58**, 1–22 (2010).
[19] E. Saglamyurek, T. Hrushevskyi, A. Rastogi, K. Heshami, and L. J. LeBlanc, "Coherent storage and manip-

ulation of broadband photons via dynamically controlled Autler–Townes splitting," Nat. Photonics **12**, 774–782 (2018).

[20] L. DiCarlo, J. M. Chow, J. M. Gambetta, Lev S. Bishop, B. R. Johnson, D. I. Schuster, J. Majer, A. Blais, L. Frunzio, S. M. Girvin, and R. J. Schoelkopf, "Demonstration of two-qubit algorithms with a superconducting quantum processor," Nature **460**, 240–244 (2009).

[21] H. J. Kimble, "The quantum internet," Nature **453**, 1023–1030 (2008).

[22] G. Kurizki, P. Bertet, Y. Kubo, K. Mølmer, D. Petrosyan, P. Rabl, and J. Schmiedmayer, "Quantum technologies with hybrid systems," Proceedings of the National Academy of Sciences **112**, 3866–3873 (2015).

[23] J. T. Hill, A. H. Safavi-Naeini, J. Chan, and O. Painter, "Coherent optical wavelength conversion via cavity optomechanics," Nat. Commun. **3**, 1196 (2012).

[24] C. Dong, V. Fiore, M. C. Kuzyk, and H. Wang, "Optomechanical dark mode," Science **338**, 1609–1613 (2012).

[25] Y. Liu, M. Davanço, V. Aksyuk, and K. Srinivasan, "Electromagnetically induced transparency and wideband wavelength conversion in silicon nitride microdisk optomechanical resonators," Phys. Rev. Lett. **110**, 223603 (2013).

[26] F. Lecocq, J. B. Clark, R. W. Simmonds, J. Aumentado, and J. D. Teufel, "Mechanically mediated microwave frequency conversion in the quantum regime," Phys. Rev. Lett. **116**, 043601 (2016).

[27] C. F. Ockeloen-Korppi, E. Damskgg, J.-M. Pirkkalainen, T. T. Heikkil, F. Massel, and M. A. Sillanp, "Low-noise amplification and frequency conversion with a multiport microwave optomechanical device," Phys. Rev. X **6**, 041024 (2016).

[28] J. Bochmann, A. Vainsencher, D. D. Awschalom, and A. N. Cleland, "Nanomechanical coupling between microwave and optical photons," Nat. Phys. **9**, 712–716 (2013).

[29] T. Bagci, A. Simonsen, S. Schmid, L. G. Villanueva, E. Zeuthen, J. Appel, J. M. Taylor, A. Sørensen, K. Usami, A. Schliesser, and E. S. Polzik, "Optical detection of radio waves through a nanomechanical transducer," Nature **507**, 81–85 (2014).

[30] K. C. Balram, M. I. Davanço, J. D. Song, and K. Srinivasan, "Coherent coupling between radiofrequency, optical and acoustic waves in piezo-optomechanical circuits," Nat. Photonics **10**, 346–352 (2016).

[31] R. W. Andrews, R. W. Peterson, T. P. Purdy, K. Cicak, R. W. Simmonds, C. A. Regal, and K. W. Lehnert, "Bidirectional and efficient conversion between microwave and optical light," Nat. Phys. **10**, 321–326 (2014).

[32] A. P. Higginbotham, P. S. Burns, M. D. Urmey, R. W. Peterson, N. S. Kampel, B. M. Brubaker, G. Smith, K. W. Lehnert, and C. A. Regal, "Harnessing electro-optic correlations in an efficient mechanical converter," Nat. Phys. **14**, 1038–1042 (2018).

[33] A. Vainsencher, K. J. Satzinger, G. A. Peairs, and A. N. Cleland, "Bi-directional conversion between microwave and optical frequencies in a piezoelectric optomechanical device," Appl. Phys. Lett. **109**, 033107 (2016).

[34] K. C. Balram, M. Davanço, J. Y. Lim, J. D. Song, and K. Srinivasan, "Moving boundary and photoelastic coupling in GaAs optomechanical resonators," Optica **1**, 414 (2014).

[35] A. J. R. MacDonald, G. G. Popowich, B. D. Hauer, P. H. Kim, A. Fredrick, X. Rojas, P. Doolin, and J. P. Davis, "Optical microscope and tapered fiber coupling apparatus for a dilution refrigerator," Rev. Sci. Instrum. **86**, 013107 (2015).

[36] S. M. Meenehan, J. D. Cohen, G. S. MacCabe, F. Marsili, M. D. Shaw, and O. Painter, "Pulsed excitation dynamics of an optomechanical crystal resonator near its quantum ground state of motion," Phys. Rev. X **5**, 041002 (2015).

[37] B. D. Hauer, P. H. Kim, C. Doolin, F. Souris, and J. P. Davis, "Two-level system damping in a quasi-one-dimensional optomechanical resonator," Physical Review B **98**, 214303 (2018).

[38] B. D. Hauer, J. Maciejko, and J. P. Davis, "Nonlinear power spectral densities for the harmonic oscillator," Ann. Phys. **361**, 148–183 (2015).

[39] J. S. Blakemore, "Semiconducting and other major properties of gallium arsenide," J. Appl. Phys. **53**, R123–R181 (1982).

[40] M. Hamoumi, P. E. Allain, W. Hease, E. Gil-Santos, L. Morgenroth, B. Gérard, A. Lemaître, G. Leo, and I. Favero, "Microscopic nanomechanical dissipation in gallium arsenide resonators," Phys. Rev. Lett. **120**, 223601 (2018).

[41] D. T. Nguyen, C. Baker, W. Hease, S. Sejil, P. Senellart, A. Lemaître, S. Ducci, G. Leo, and I. Favero, "Ultrahigh q-frequency product for optomechanical disk resonators with a mechanical shield," Appl. Phys. Lett. **103**, 241112 (2013).

[42] Biswarup Guha, Felix Marsault, Fabian Cadiz, Laurence Morgenroth, Vladimir Ulin, Vladimir Berkovitz, Aristide Lemaître, Carmen Gomez, Alberto Amo, Sylvain Combrié, Bruno Gérard, Giuseppe Leo, and Ivan Favero, "Surface-enhanced gallium arsenide photonic resonator with quality factor of 6×10^6 " Optica **4**, 218 (2017).

[43] C. P. Michael, K. Srinivasan, T. J. Johnson, O. Painter, K. H. Lee, K. Hennessy, H. Kim, and E. Hu, "Wavelength- and material-dependent absorption in GaAs and AlGaAs microcavities," Applied Physics Letters **90**, 051108 (2007).

[44] M. L. Gorodetsky, A. Schliesser, G. Anetsberger, S. Deleglise, and T. J. Kippenberg, "Determination of the vacuum optomechanical coupling rate using frequency noise calibration," Opt. Express **18**, 23236 (2010).